NANO LETTERS
Letter
Cite This: Nano Lett. 2018, 18, 5797−5804
pubs.acs.org/NanoLett

In Vivo Mitigation of Amyloidogenesis through Functional−Pathogenic Double-Protein Coronae

Ibrahim Javed,[†,‡] Tianyu Yu,[‡] Guotao Peng,[‡] Antoni Sánchez-Ferrer,[§] Ava Faridi,[†] Aleksandr Kakinen,[†] Mei Zhao,[‡] Raffaele Mezzenga,[§] Thomas P. Davis,*[,†] Sijie Lin,*[,‡] and Pu Chun Ke*[,†]

[†]ARC Centre of Excellence in Convergent Bio-Nano Science and Technology, Monash Institute of Pharmaceutical Sciences, Monash University, 381 Royal Parade, Parkville, Victoria 3052, Australia

[‡]Biomedical Multidisciplinary Innovation Research Institute, Shanghai East Hospital, State Key Laboratory of Pollution Control and Resource Reuse, Shanghai Institute of Pollution Control and Ecological Security, College of Environmental Science and Engineering, Tongji University, 1239 Siping Road, Shanghai 200092, China

[§]Department of Health Sciences & Technology, ETH Zurich, Schmelzbergstrasse 9, LFO, E23, 8092 Zurich, Switzerland

Supporting Information

ABSTRACT: Amyloid diseases are global epidemics with no cure available. Herein, we report a first demonstration of in vivo mitigation of amyloidogenesis using biomimetic nanotechnology. Specifically, the amyloid fragments (b_a) of β-lactoglobulin, a whey protein, were deposited onto the surfaces of carbon nanotubes (b_aCNT), which subsequently sequestered human islet amyloid polypeptide (IAPP) through functional-pathogenic double-protein coronae. Conformational changes at the b_a−IAPP interface were studied by Fourier transform infrared, circular dichroism, and X-ray scattering spectroscopies. b_aCNT eliminated the toxic IAPP species from zebrafish embryos, as evidenced by the assays of embryonic development, cell morphology, hatching, and survival as well as suppression of oxidative stress. In addition to IAPP, b_aCNT also displayed high potency against the toxicity of amyloid-β, thereby demonstrating the broad applicability of this biomimetic nanotechnology and the use of an embryonic zebrafish model for the high-throughput screening of a range of amyloidogenesis and their inhibitors in vivo.

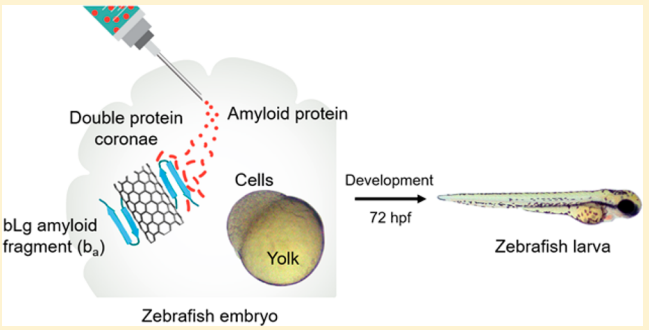

KEYWORDS: *Amyloidogenesis, IAPP, amyloid β, zebrafish, carbon nanotubes, amyloid diseases*

Amyloid diseases are modern epidemics that impact more than 6% of the global population and are characterized by deposits of amyloid fibrils and plaques in the brain and pancreas as well as other bodily organs.[1] The development of such aberrant biological substances is consequential to the fibrillization of amyloid proteins such as amyloid-β (Aβ), associated with Alzheimer's disease, and human islet amyloid polypeptide (IAPP), associated with type 2 diabetes (T2D), from the nucleation of monomers into oligomers and the elongation of oligomers into amyloid fibrils. Regardless of their physiological and pathological origins, the oligomeric forms of amyloid proteins are believed to be the major toxic species.[2,3] Such oligomers show a propensity of partitioning in lipid membranes in a porin-like fashion to alter the fluidity and integrity of the cell.[4,5] Amyloid fibrils, in addition, can extract lipids from membranes through hydrophobic interactions.[6] The fibrillization of amyloid proteins, furthermore, has been found to stimulate the production of reactive oxygen species (ROS) to trigger cell degeneration.[1]

A common mitigation strategy against amyloidogenesis is to minimize the population of the toxic oligomeric species by pitching protein-inhibitor interaction against protein−protein interaction.[7−10] Hydrogen bonding and hydrophobic interaction as well as the π stacking of cross-β amyloid proteins are not only responsible for the self-assembly but also postulated as a reason for the cross-talk between pathogenic--pathogenic or functional--pathogenic amyloid proteins.[11−13] Such interactions have recently been exploited for the development of theranostics against amyloidogenesis,[10] the construction of three-dimensional nanoarchitectures,[14] and cross-talk between pathogenic amyloid proteins in which parent seeds transferred the toxic and structural polymorphs to daughter fibrils.[15,16]

β-Lactoglobulin (bLg) is a functional whey protein that, under high temperature and low pH, self-assembles into amyloid fibrils of similar morphology to that of IAPP or Aβ.[17] This class of functional amyloid has shown potential as versatile substrates or scaffolds for tissue engineering, iron fortification, and water purification.[18−20] To exploit the cross-talk and medicinal

Received: June 16, 2018
Revised: August 5, 2018
Published: August 8, 2018

Downloaded via MONASH UNIV on September 12, 2018 at 06:53:55 (UTC).
See https://pubs.acs.org/sharingguidelines for options on how to legitimately share published articles.

© 2018 American Chemical Society

DOI: 10.1021/acs.nanolett.8b02446
Nano Lett. 2018, 18, 5797−5804

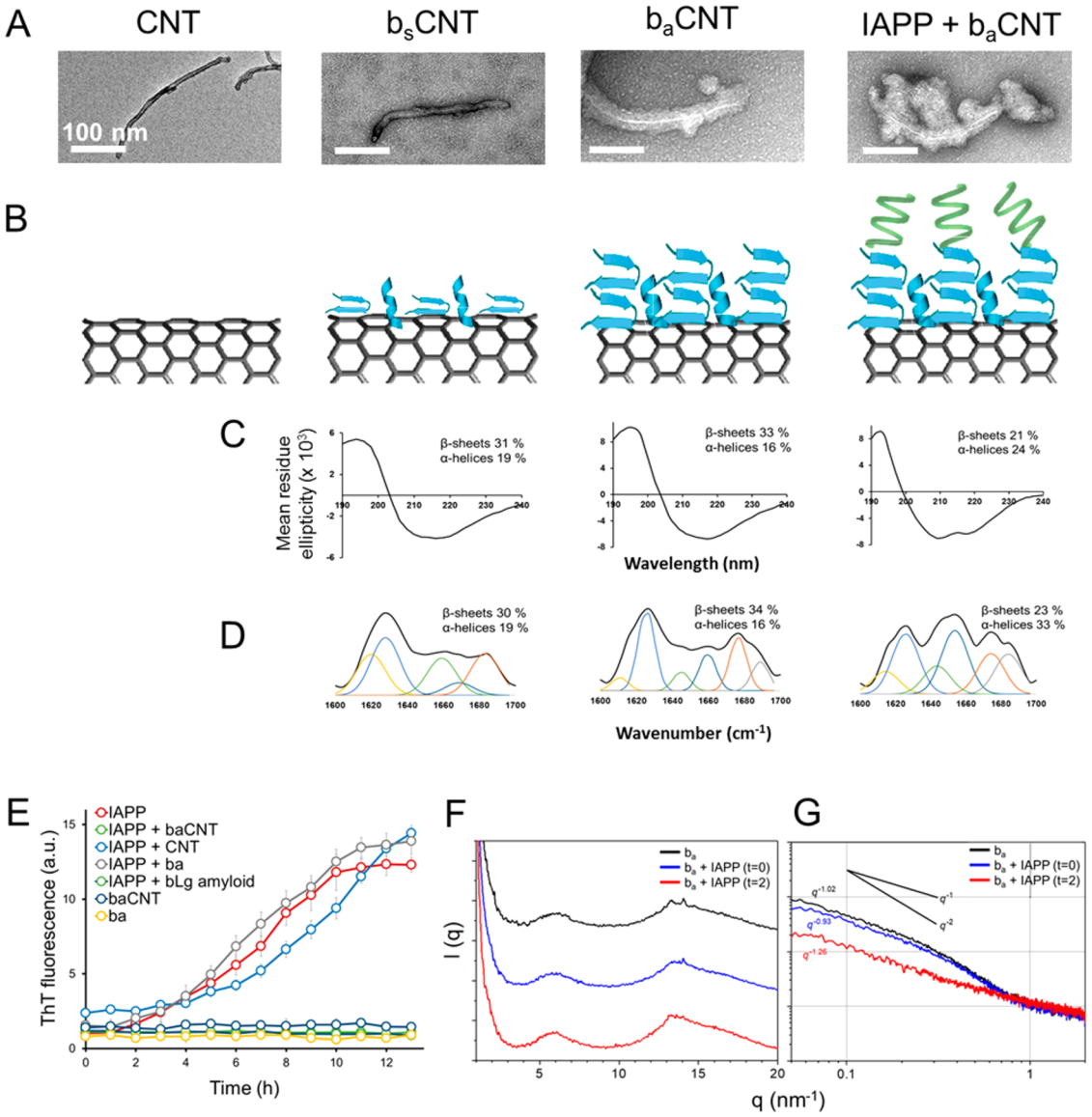

Figure 1. Synthesis scheme of CNTs functionalized with bLg amyloid corona, their surface properties, and interaction with IAPP in fibrillization. (A) TEM images of the synthesized materials and their associations with IAPP. Pristine multiwalled carbon nanotubes (CNTs) of 10−20 nm diameter were sonicated with bLg amyloid fragments (b_a). Sonication deposited an initial layer of ∼10 nm on the CNTs (b_sCNT) and stabilized their dispersion in water. Further heating of this dispersion resulted in coalescence of surrounding b_a on the CNT surfaces, resulting in a b_a corona of ∼30−50 nm on the b_aCNT surfaces. b_aCNT further captured IAPP in the form of small protruding aggregates. Scale bars: 100 nm. (B) Graphical illustration of the materials preparations. The structures of the coronae were studied with (C) CD spectroscopy and (D) FTIR amide-I band deconvolution, revealing that a relatively larger proportion of β-sheet rich corona was imparted by b_a on the CNT surfaces. After the sequestering of IAPP, the overall secondary structure of the corona was shifted toward the α helix. (E) ThT kinetic assay revealed complete inhibition of IAPP (50 μM) fibrillization by b_aCNT (50 μM with respect of b_a). CNTs and b_a inhibited IAPP fibrillization, and no ThT fluorescence was observed in the controls of b_aCNTs or b_a alone. (F) WAXS intensity profiles of dry samples of b_a, b_a plus IAPP (t = 0 h), and b_a plus IAPP (t = 2 h). (G) SAXS intensity profiles of the water dispersions of b_a, b_a plus IAPP (t = 0 h), and b_a+ IAPP (t = 2 h).

potentials of functional bLg amyloid, we interfaced bLg amyloid fragments (abbreviated as b_a) with IAPP to capture the toxic IAPP species for mitigating IAPP amyloidogenesis in vivo. Multiwalled carbon nanotubes (CNTs) were employed as a model hydrophobic substrate to host a b_a layer, or a protein "corona",[21] on the tube surfaces via hydrophobic interaction and π stacking. The nonspecific binding of CNTs and Aβ has been previously examined in silico, in which the protein β-sheets wrapped around the CNT surfaces to reduce the latter's surface energy in the aqueous phase.[22] Such coronae afforded by proteins and other natural amphiphiles provided both the ability to suspend in water and a new biological identity to their carbon-based nanomaterial substrates.[23,24]

In the present study, the biomimetic constructs of a b_a corona adsorbed on a CNT surface (b_aCNT) displayed a high portion of β-sheets, which subsequently inhibited toxic IAPP species at the early stage of IAPP fibrillization. As a high-throughput model system, zebrafish embryos were developed and comprehensively characterized for screening the toxicities of amyloid proteins IAPP and Aβ as well as their mitigation by b_aCNT. This study first demonstrated the feasibility of in vivo mitigation of amyloidogenesis with a facile biomimetic nanotechnology and the use of a nanoliter sample volume for the induction of

DOI: 10.1021/acs.nanolett.8b02446
Nano Lett. 2018, 18, 5797−5804

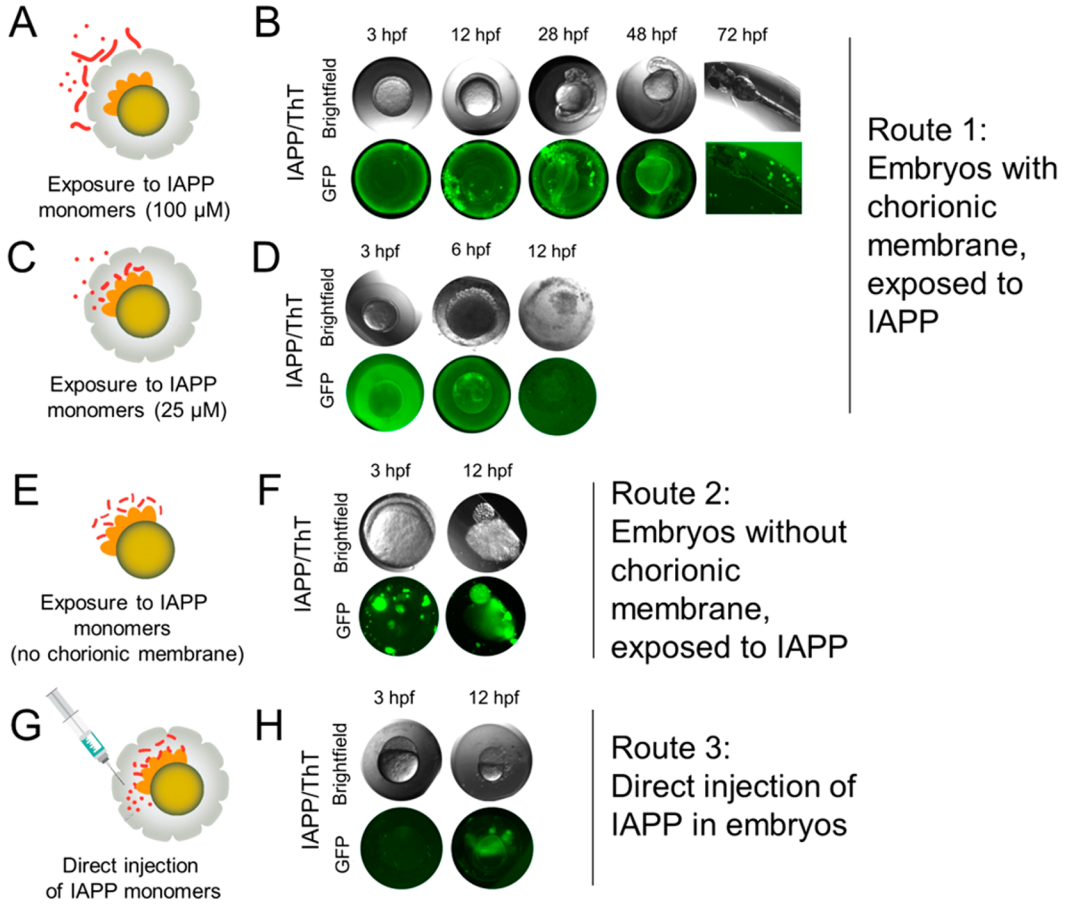

Figure 2. Toxicity of IAPP fibrillization in zebrafish embryos. IAPP peptide monomers were exposed to zebrafish embryos via three different routes, and embryonic development was monitored in the bright-field and GFP channel of a fluorescence microscope until successful hatching on the fourth day. Controls of embryos injected with equal amounts of ThT presented no fluorescence. (A) Exposure of a zebrafish embryo with chorionic membrane to IAPP of 100 μM. (B) IAPP aggregated on the membranes without penetrating through the chorionic pores. To induce peptide−chorion interaction, (C) IAPP concentration was decreased to 25 μM in the outer solution, and (D) ThT fluorescence indicated penetration of IAPP into the perivitelline space. (E) In the case of unprotected embryos, (F) IAPP induced toxicity within the first 12 h of development. (G) Direct injection of IAPP into the perivitelline space of embryos bypassed the chorionic barrier and resulted in direct interactions of the peptide with the lipid membranes of cells, as indicated by (H) ThT fluorescence and the toxic arrest of embryonic development at 12 hpf.

amyloid protein toxicity, two major technical advancements for the rapid screening of amyloidogenesis and their inhibitors toward a cure for amyloid diseases.[1]

Sonicated bLg amyloid fragments (b_a) were adsorbed on the CNT (~20 nm in diameter) surfaces to render a protein corona of ~30 ± 5 nm (Figure 1A). The elemental composition of pristine CNTs was determined by X-ray photoelectron spectroscopy (XPS), which contained mostly carbon (97.2%) as well as small traces of impurities of O (2.6 ± 0.1%) and Si (0.2 ± 0.0%). bLg amyloids were first synthesized by overnight heating (80 °C, pH 2) of 2% aqueous solution of bLg monomers, and the amyloid fibrils were then broken down to small fragments by probe sonication (Figure S1). The CNTs were embedded inside a thick coat of b_a in a two-step process: first, a layer of ~10 ± 3 nm of b_a was deposited on the CNTs by sonication (b_sCNT), and subsequent heating (70 °C for 30 min at pH 4.3) grew the initial layer to ca. 50 ± 7 nm, resulting in b_aCNT (Figure 1A,B). The sizes of the CNTs before and after deposition of the b_a corona were measured directly from transmission electron microscopy (TEM). Sonication exposed the hydrophobic cores of the protein species, b_s in this case, to facilitate their binding with the hydrophobic CNTs,[25] while heating induced free proteins in the solution to coalesce on the already adsorbed protein layer, increasing the protein content on the CNT surfaces from 67% to 76% for b_aCNT (Figure S2A). Dynamic light scattering (DLS) revealed that the hydrodynamic radius of b_aCNT was increased by ~9 nm from b_sCNT after heating (Table S1). The protein secondary structure of the b_a corona was estimated by circular dichroism (CD) and Fourier transform infrared (FTIR) spectroscopies, revealing a β-sheet content of 33−34% (Figure 1C,D), comparable to that of bLg amyloid (~40%)[10,26] prior to sonication and deposition onto CNTs. The thickening of b_sCNT into b_aCNT by heating did not induce major effects on the secondary structure of the b_a corona.

A thioflavin T (ThT) kinetic assay revealed that b_aCNT completely inhibited IAPP fibrillization at equimolar concentrations (for IAPP and b_a) (Figure 1E). Changes in the b_aCNT surface charge indicated the adsorption and physical state of IAPP on the CNTs. Specifically, the ζ potential for IAPP peptide and mature fibrils was +15.8 and +65.3 mV, respectively. Upon incubation with IAPP, the ζ potential of b_aCNT changed from −18.4 to −12.5 mV (Table S1), indicating association of cationic IAPP with b_aCNT. CD and FTIR spectra revealed that IAPP assumed a β-sheet rich conformation upon fibrillization (Figure S2B,C). When incubated with IAPP, large protruding aggregates of IAPP were observed on the b_aCNT surfaces by

DOI: 10.1021/acs.nanolett.8b02446
Nano Lett. 2018, 18, 5797−5804

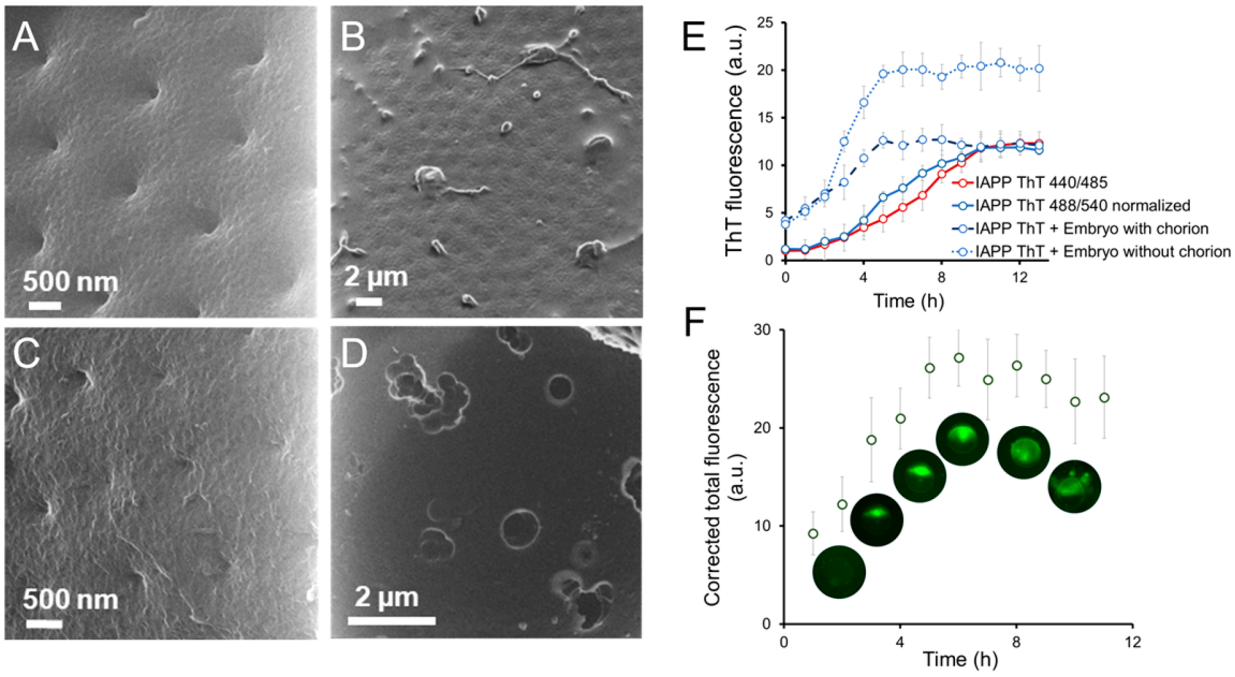

Figure 3. Amyloidogenic interactions and fibrillization kinetics of IAPP with zebrafish embryos. (A–D) IAPP–embryonic interactions were examined by helium-ion microscopy (HIM). (A) When embryos were developed in IAPP of 25 μM, IAPP trespassed through the pores of chorionic membranes. (B) In the presence of IAPP of 100 μM, the peptide aggregated on the outer surfaces of the embryos. (C) In contrast, unobstructed clear pores can be seen in control embryos. (D) The chorionic membrane of an embryo was cut open to assess IAPP interacting with the underlying embryonic cell. IAPP toxicity is indicated by morphological changes in the embryonic cellular membrane. (E) ThT kinetic assay of IAPP fibrillization in the presence of embryos, with and without chorionic membranes, i.e., the first and second routes of exposure. IAPP: 25 μM; ThT: 50 μM. The shape of ThT kinetic curve (excitation/emission: 440 nm/485 nm) recorded on a plate-reader is comparable to that acquired via the GFP channel (excitation/emission: 488 nm/540 nm). The ThT fluorescence intensity in the GFP channel was normalized by multiplying by a factor of 5 for the comparison. (F) fibrillization kinetics of IAPP with the third route of exposure (direct injection) was measured by microinjecting 5 nL of IAPP (50 μM) and ThT (100 μM) inside embryos.

TEM (Figure 1A), rendering an elevated α-helix content compared to that of b_aCNT (Figure 1C,D). It has been shown in the literature that protein or lipid interfaces can trigger conformational changes or oligomerization in the adsorbed protein.[27,28] Sonication and heat-induced adsorption of b_a on the CNTs exposed their hydrophobic cores,[29,30] while IAPP bound b_aCNT via hydrogen bonding and hydrophobic interaction, converting the protein from random coils to the α-helical conformation (Figure S2B,C versus Figure 1C,D). This is in contrast to our previous study,[10] in which spherical gold nanoparticles (AuNPs, 5 nm) coated by b_a intercalated inside IAPP fibrils during fibrillization. This difference may be attributed to the significantly different morphologies and aspect ratios of CNTs (>25) and AuNPs (~1). It is conceivable that b_a on the tubular CNT substrate assumed more directional orientations than on spherical AuNPs, thereby allowing surface adsorption of disordered IAPP monomers but preventing that of cross-β IAPP protofibrils from inhibiting IAPP fibrillization.

To assess how IAPP might affect the structure of b_a, a wide-angle X-ray scattering (WAXS) experiment was performed on dry samples containing b_a (without CNTs) after the immediate addition of IAPP (b_a-IAPP at t = 0) and 2 h of incubation (b_a-IAPP at t = 2). Samples containing b_a displayed two peaks characteristic of inter and intra β-sheet distances at q = 6.0 and 13.4 nm^{-1} ($d_{\beta\text{-sheet}}$ = 1.1 nm and $d_{\beta\text{-strand}}$ = 4.7 Å, respectively) (Figure 1F). No differences due to the presence of CNTs were observed on the β-sheet secondary structure from the WAXS analysis (Figure S3A). Thus, no major changes at the molecular level were observed in b_a after the addition of IAPP.

Additionally, small-angle X-ray scattering (SAXS) experiment was conducted on water dispersions containing b_a, after immediate introduction of IAPP (b_a-IAPP at t = 0) and 2 h of incubation (b_a-IAPP at t = 2). No differences due to the presence of CNTs were observed on the β-sheet secondary structure from the SAXS analysis (Figure S3B). No significant changes in the scattering profiles were observed between the genitor samples and after adding IAPP at 0 h (Figure 1G). After 2 h of incubation with IAPP, b_a exhibited different SAXS intensity profiles compared with the corresponding genitor systems. This indicates that IAPP interacted with the bLg species (tubular β sheets) building up different colloidal particles but maintaining the initial secondary structures.

The recent failure of the phase-3 trial of solanezumab at Eli Lilly and the general lack of clinical success in the field of amyloidogenesis may be partially attributed to a deficiency in antiamyloidogenesis strategies and a lack of easily accessible, economic in vivo models.[31] Zebrafish (*Danio rerio*) share 70% of their genome and 84% of their disease-related genes with humans and are a preeminent vertebrate model for toxicology, pharmacology, and genetics research.[32] Zebrafish larvae display neuropathological and behavioral phenotypes that are quantifiable and relate to those seen in humans and have been applied to many studies of Huntington's, Alzheimer's, and Parkinson's diseases.[33,34] Here, we first developed zebrafish embryos as an in vivo model for screening nanoscale inhibitors against amyloid protein toxicity. The fibrillization and interaction of IAPP with zebrafish embryos were tracked by tagging the IAPP protofibrils and fibrils with the β-sheet affinitive ThT dye and visualized

DOI: 10.1021/acs.nanolett.8b02446
Nano Lett. 2018, 18, 5797–5804

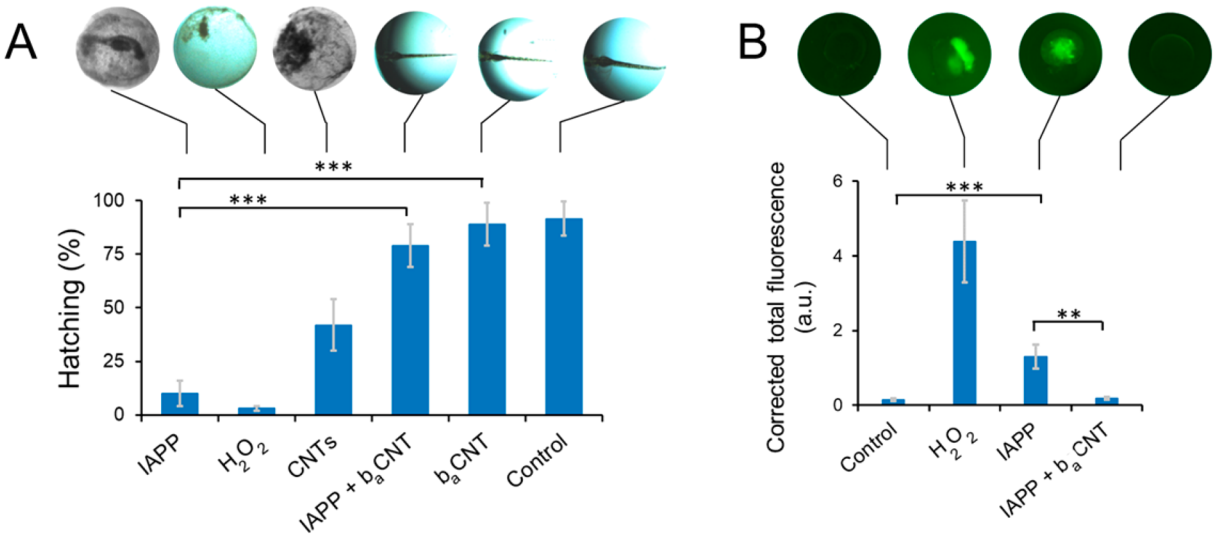

Figure 4. IAPP toxicity mitigation via functional-pathogenic double coronae on CNTs. (A) IAPP along with b_aCNT were injected inside zebrafish embryos and mitigation of IAPP toxicity was observed in terms of hatching survival of embryos on the third day post fertilization (72 hpf). b_aCNT protected the embryos from IAPP toxicity (triple asterisks indicate $p < 0.005$), while b_aCNT were biocompatible with the embryos and induced no toxicity. (B) ROS assay further confirmed the oxidative stress resulted from IAPP interaction with embryos and its mitigation by b_aCNT. ROS generation by IAPP was significantly higher than the control.

under the green fluorescence protein (GFP) channel of a fluorescence microscope (Figure S4). To determine the optimal method for assessing IAPP toxicity, zebrafish embryos were exposed to IAPP monomers via three different routes, and their efficacies were assessed.

First, embryos (3 h post-fertilization, hpf) were developed with intact chorionic membranes in 100 μM of IAPP solution (Figure 2A). When traced by ThT (100 μM), IAPP was found to aggregate on the surfaces of chorionic membranes and was unable to penetrate through the chorionic pores. Therefore, no toxicity was observed in the embryos (Figure 2B). However, when embryos with chorionic membranes were developed in IAPP solution of 25 μM (Figure 2C), the peptide penetrated through the chorionic membranes to interact with the underlying embryonic cells to induce toxicity (Figure 2D). Compared to an IAPP of 100 μM, in which peptide−peptide interaction was dominant to form aggregates, peptide−chorion interaction was evident at IAPP of 25 μM in concentration, showing diffused ThT fluorescence in the perivitelline space at 3 hpf. Fibrillizing IAPP interacted with the underlying embryos at 6 hpf and toxic arrest of embryonic development was observed at 12 hpf (Figure 2D).

In the second route of exposure, embryos without chorionic membranes were developed in IAPP solution of different concentrations (Figure 2E). The IC_{50} value of IAPP was reduced to 25 ± 12.5 μM, as assessed by the percent hatching of the embryos on the third day post-fertilization (dpf). Fibrillating IAPP interacted with the cellular mass of the embryos immediately after mixing (Figure 2F). At 12 hpf, the dividing cells inside the embryos shrank to small globular masses, and the embryos lost viability. Strong ThT fluorescence, indicating IAPP amyloid aggregation, was associated with dead embryonic cells resulting from their exposure to IAPP.

In the third route of exposure, different concentrations of IAPP (5 nL of 2 to 100 μM) were directly injected inside the perivitelline space of embryos (Figure 2G). The IC_{50} value of IAPP was found to be 5.6 ± 1.7 μM, the lowest for the three routes of exposure. ThT fluorescence indicated that IAPP aggregated on the lipid membranes of the embryonic cells (Figure 2H, fluorescence image on the right) and toxic arrest of embryonic development was observed at 12 hpf.

Helium ion microscopy (HIM) was used to further visualize the interaction of IAPP with chorion and lipid membranes of embryonic cells. HIM imaging of zebrafish chorions revealed a porous morphology with an average pore size of ∼200 nm (Figure 3A), which led to the hypothesis that IAPP monomers could penetrate through the pores to induce toxicity to the underlying embryonic cells. In the first route of exposure, in which IAPP was exposed to embryos with chorionic membranes, IAPP of 100 μM in concentration formed large fibrillary aggregates outside the membrane pores and was not able to penetrate (Figure 3B). However, at an IAPP concentration of 25 μM, the chorionic pores were less visible due to trespassing IAPP aggregates (Figure 3C). To visualize the interaction of IAPP with the lipid membranes of underlying embryonic cells, which is relevant to the second and third routes of IAPP administration, embryos treated with the direct micro-injection of IAPP were cut open to reveal the embryonic cells. IAPP elicited toxicity to the embryonic cells, as evidenced in the form of holes, swelling, and morphological irregularities in the membranes (Figure 3D).

The IAPP fibrillization kinetics for the three routes of exposure was recorded. In the first case, the chorionic membranes significantly enhanced the fibrillization (50 μM IAPP) and shortened the lag time. However, the saturation phase remained the same as the control (Figure 3E). This is understandable because polysaccharides are the major component of zebrafish chorions and have been previously observed to accelerate oligomerization of α-synuclein and Aβ.[35,36] In the second case of no chorion, exposure of the lipid membranes of embryonic cells to IAPP resulted in faster fibrillization and a higher saturation plateau, suggesting consumption of available monomers or oligomeric seeds and early formation of mature fibrils (Figure 3E).[37] In the third case of direct injection, IAPP monomers (12.5 μM) and ThT (25 μM) were microinjected inside the perivitelline space of embryos to observe IAPP

DOI: 10.1021/acs.nanolett.8b02446
Nano Lett. 2018, 18, 5797−5804

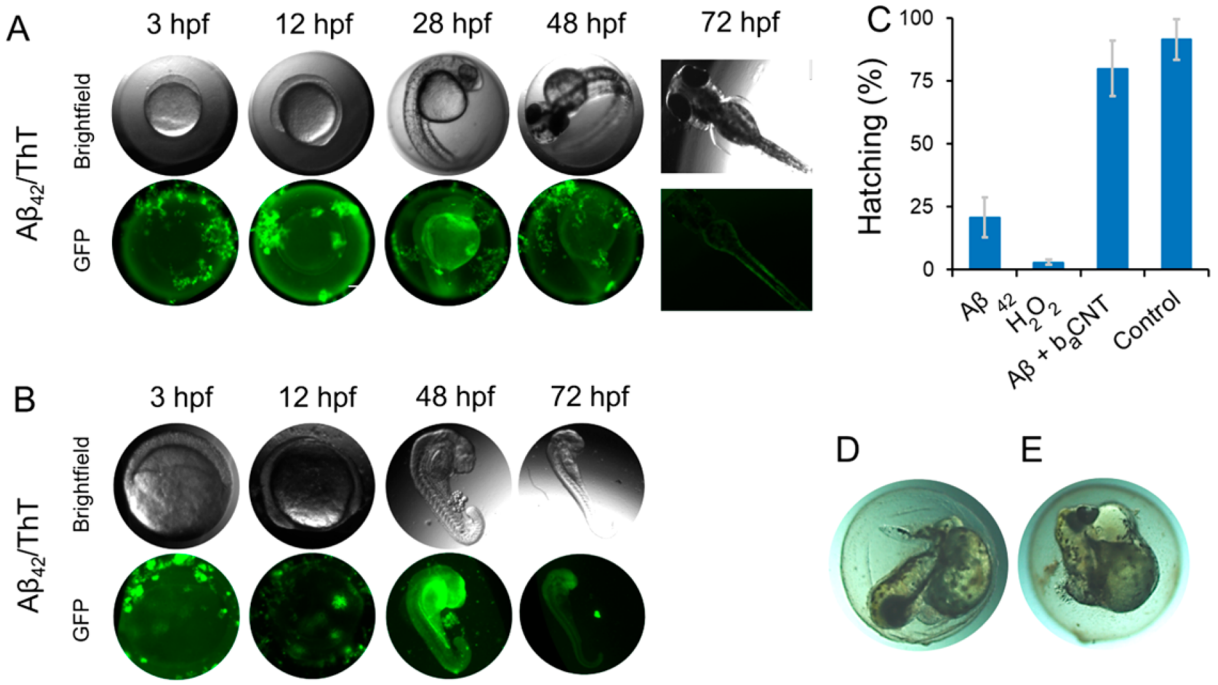

Figure 5. Aβ toxicity mitigation via functional-pathogenic double coronae on CNTs. Development of embryo was monitored (A) with and (B) without chorionic membrane inside a solution of fibrillating Aβ42. Similar to IAPP, Aβ was not able to penetrate through the chorionic pores at a 100 μM concentration. However, the IC_{50} value of Aβ was 100 ± 25 μM when embryos were directly exposed to Aβ solution. (C) b_aCNTs were able to sequester the toxicity of Aβ in the embryo. (D, E) Phenotypically strange development was observed for the embryo when injected with sub-toxic concentration (5 μM) of Aβ.

fibrillization kinetics inside the chorionic fluids (Figure 3E). The saturation phase was reached at ~6 h for all three cases. Overall, the third route of exposure appeared to be the most efficient with sample volume (5 nL) and most facile in terms of execution (i.e., microinjection of samples directly into the perivitelline space of embryos).

The interaction between mature IAPP fibrils and developing zebrafish embryos was also studied by injecting the ThT-tagged fibrils (100 μM of both IAPP and ThT, 24 h of maturation) inside the perivitelline space of embryos at 3 hpf (Figure S5A). No toxicity was observed based on the development and survival of the embryos (Figure S5B). The development of the embryos treated with IAPP fibrils was comparable to the control. However, hatching was significantly delayed by 48 ± 5 h compared to the control, suggesting a possible interaction between IAPP fibrils and the hatching enzyme, a zinc metalloprotease.[38] This is plausible because metals, especially zinc, interact strongly with IAPP to alter the latter's fibrillization and toxicity.[39,40] In comparison, no fluorescence was observed for control embryos microinjected with ThT (Figure S5B).

Peptide-based inhibitors have shown efficacies in the inhibition of IAPP aggregation both in vitro and with transgenic animal models.[41−47] bLg amyloids are functional and biocompatible and yet possess a similar morphology as IAPP fibrils;[10,18] hence, they may serve as an inhibitor against IAPP toxicity. However, in vivo administration of full-length bLg amyloids is unfeasible due to their large dimensions (micrometers in length) compared to blood vasculature, and b_a itself did not elicit a notable inhibitory effect on IAPP fibrillization (Figure 1E). Accordingly, b_a was stabilized on CNT surfaces in this study, simultaneously improving the biocompatibility of CNTs while enabling inhibitory interaction with IAPP. The embryonic zebrafish system was employed to translate the mitigation potential of b_aCNT against IAPP toxicity in vivo. Direct microinjection (route 3) was adopted because this mode of exposure allowed the use of ultrasmall sample volumes without the interference from chorionic membranes. b_aCNT were injected together with IAPP at equimolar concentrations of 10 μM (i.e., higher than the IC_{50} value of 5.7 μM). b_aCNT eliminated IAPP toxicity and restored the hatching survival of IAPP-treated embryos to 85%, while b_aCNT themselves displayed no toxicity to the embryos (Figure 4A).

The above toxicity study was augmented by a ROS assay (Figure 4B). Specifically, IAPP monomers were mixed with 2′,7′-dichlorodihydrofluorescein diacetate (H_2DCFDA) dye, immediately before being microinjected into the perivitelline space. ROS generation, resulting from membrane disruption of embryonic cells, was observed for IAPP. However, consistent with the hatching survival assay, no ROS species were detected when IAPP was incubated with b_aCNT.

To evaluate the mitigation potential of b_aCNT, Aβ was introduced to elicit toxicity in zebrafish embryos. Similar to IAPP, fibrillating Aβ (100 μM) was not able to penetrate through the chorionic pores of embryos but aggregated on chorionic membranes (Figure 5A). However, when chorionic membranes were removed and embryos were exposed, Aβ of 100 ± 25 μM was toxic to the embryos. In comparison to IAPP, the fibrillization of Aβ was slower, and the embryos survived the 3rd through the 6th somite stages at 12 hpf, after which the embryo development was arrested at the 20th somite stage at 48 hpf, and ThT fluorescence was observed from the anterior of the larvae (Figure 5B). The IC_{50} value of Aβ, when injected directly inside the perivitelline space, was determined to be 7.4 ± 0.84 μM. In comparison, Donnini et al. reported a cerebral angiopathic effect of wild-type Aβ peptide in zebrafish embryos at 2.5 μM, in which the IC_{50} value was determined to be 6.1 μM,

DOI: 10.1021/acs.nanolett.8b02446
Nano Lett. 2018, 18, 5797−5804

comparable to that determined by our current approach.[48] b_aCNT were then injected together with Aβ at equimolar concentrations of 15 μM (i.e., higher than the MIC values), and b_aCNT rescued ($p < 0.005$) the embryos from Aβ toxicity (Figure 5C). Abnormal phenotypic development of embryos was observed, when the embryos were microinjected with Aβ at 5 μM that was just below the IC_{50} value (Figure 5D,E), which can explain well the Aβ-induced neurovascular degeneration and cerebral senescence observed by Donnini et al.[48] These agreements with literature further validated our current methodologies. It should be noted that the functional−pathogenic double protein coronae on CNTs, as delineated for the in-solution characterizations (Figure 1B), do not encompass all possible protein−protein interactions under in vivo conditions, in which the chorionic sac also contained zebrafish hatching enzyme 1 (ZHE1), glycoprotein subunits, and different forms of metabolites during embryonic development.[49−52] However, because b_a was rich in β-sheets and therefore possessed a higher affinity for amyloid proteins,[10,53,54] the binding of b_a with IAPP through H-bonding and hydrophobic and electrostatic interactions as well as β-sheet stacking should dominate the nonspecific interactions ("soft corona") between b_a and the other proteins and enzymes. This robust mitigation potential of b_aCNT against amyloid proteins was corroborated by additional ThT and viability assays (Figure S6), in which the presence of human plasma proteins and fetal bovine serum (FBS) did not compromise the potency of b_aCNT from inhibiting IAPP aggregation and toxicity. This latter aspect also points to the promise of exploiting the b_aCNT nanotechnology in biological fluids beyond the chorionic sac.

In summary, we have developed a facile, potent biomimetic nanotechnology against amyloidogenesis in vivo. This nanotechnology consisted of CNTs coated with a cross-β-sheet-rich, functional corona of whey protein bLg amyloid fragments (b_a), which consequently acquired a pathogenic protein corona by sequestering amyloid protein IAPP or Aβ. No IAPP fibrillization inhibition was observed for b_a alone (Figure 1E), justifying the role of the CNT substrates in orienting the adsorbed amyloid fragments and subsequently capturing the pathogenic protein from on-pathway fibrillization. In contrast to b_aCNT, bLg monomer-coated CNTs (b_mCNT) (Figure S7A), possessing no cross-β-sheet component, displayed a much-lower efficiency in inhibiting IAPP fibrillization (Figure S7B versus Figure 1E). In addition, an embryonic zebrafish assay through direct microinjection, i.e., the third route of exposure, has been developed into a high-throughput platform for screening amyloidogenesis and its mitigation by b_aCNT in vivo. Consistent with the ThT assay, b_mCNT, being nontoxic itself (Figure S8A), was not able to rescue zebrafish embryos from the toxicity elicited by IAPP, as evidenced by both the hatching and the ROS assays (Figure S8A,B versus Figure 4). This further vindicates the crucial role of the cross-β component in b_a and the architecture of b_aCNT in effective amyloidogenesis mitigation. Other major advantages of this assay include high fecundity and transparency of the zebrafish organism as well as an ultra-small sample volume (5 nL). IAPP at high concentrations was dominated by peptide−peptide interaction, and no toxicity was induced to zebrafish embryos. Reducing the peptide concentration promoted peptide−chorion interaction, and the peptide penetrated through the chorionic pores to elicit toxicity to embryonic cells through continued aggregation. This embryonic model system is therefore suited for examining amyloidogenesis with realistic dosage. b_aCNT protected zebrafish embryos from the toxicities of both IAPP and Aβ, as evidenced by hatchling-survival and ROS-generation assays. Together, this study opens the door to the rapid screening of the toxicities of a wide range of amyloid proteins and facilitates the development of potent, bioinspired nanotechnologies[55−57] against amyloidogenesis in vivo.

■ ASSOCIATED CONTENT

Supporting Information

The Supporting Information is available free of charge on the ACS Publications website at DOI: 10.1021/acs.nanolett.8b02446.

Additional details of experimental methods. Figures showing additional TEM, TGA, WAXS and SAXS, ThT, viability, and IAPP embryonic assay data. A table showing ζ-potential and dynamic light scattering data. (PDF)

■ AUTHOR INFORMATION

Corresponding Authors

*E-mail: thomas.p.davis@monash.edu. Phone: +61-03-99039260.
*E-mail: lin.sijie@tongji.edu.cn. Phone: +86-21-65982325.
*E-mail: pu-chun.ke@monash.edu. Phone: +61-03-99039267.

ORCID

Ibrahim Javed: 0000-0003-1101-5614
Raffaele Mezzenga: 0000-0002-5739-2610
Thomas P. Davis: 0000-0003-2581-4986
Sijie Lin: 0000-0002-6970-8221
Pu Chun Ke: 0000-0003-2134-0859

Author Contributions

P.C.K., I.J., S.L., and T.P.D. designed the project. I.J. and P.C.K. wrote the manuscript. I.J. performed syntheses, CD, FTIR, ThT, TGA, XPS, ζ potential, and DLS measurements and analyses. I.J., T.Y., G.P., M.Z., and S.L. developed and performed the embryonic assays. A.S.F. and R.M. performed SAXS and WAXS experiments and analyses. A.K. and I.J. conducted TEM and prepared the illustrations. A.F. performed the cell culture and viability assay. All authors agreed on the presentation of the manuscript.

Notes

The authors declare no competing financial interest.

■ ACKNOWLEDGMENTS

This work was supported by ARC project no. CE140100036 and the Recruitment Program of "1000plan Youth" and Startup Funds from Tongji University (Lin). T.P.D. is thankful for the award of an ARC Australian Laureate Fellowship. I.J. acknowledges the support of Monash International Postgraduate Research Scholarship (MIPRS). TEM imaging was performed at Bio21 Advanced Microscopy Facility, University of Melbourne. HIM imaging was performed at the MCFP platform, University of Melbourne by Dr. Babak Nasr. I.J. and S.L. thank the Shanghai Science and Technology Commission "Belt and Road" initiative program, grant no. 17230743000.

■ REFERENCES

(1) Ke, P. C.; Sani, M.-A.; Ding, F.; Kakinen, A.; Javed, I.; Separovic, F.; Davis, T. P.; Mezzenga, R. *Chem. Soc. Rev.* **2017**, *46* (21), 6492−6531.

DOI: 10.1021/acs.nanolett.8b02446
Nano Lett. 2018, 18, 5797−5804

(2) Cao, P.; Abedini, A.; Wang, H.; Tu, L.-H.; Zhang, X.; Schmidt, A. M.; Raleigh, D. P. *Proc. Natl. Acad. Sci. U. S. A.* **2013**, *110* (48), 19279−19284.
(3) Haataja, L.; Gurlo, T.; Huang, C. J.; Butler, P. C. *Endocr. Rev.* **2008**, *29* (3), 303−316.
(4) Ritzel, R. A.; Meier, J. J.; Lin, C.-Y.; Veldhuis, J. D.; Butler, P. C. *Diabetes* **2007**, *56* (1), 65−71.
(5) Kayed, R.; Sokolov, Y.; Edmonds, B.; McIntire, T. M.; Milton, S. C.; Hall, J. E.; Glabe, C. G. *J. Biol. Chem.* **2004**, *279* (45), 46363−46366.
(6) Sparr, E.; Engel, M. F.; Sakharov, D. V.; Sprong, M.; Jacobs, J.; de Kruijff, B.; Höppener, J. W.; Antoinette Killian, J. *FEBS Lett.* **2004**, *577* (1−2), 117−120.
(7) Cabaleiro-Lago, C.; Lynch, I.; Dawson, K.; Linse, S. *Langmuir* **2010**, *26* (5), 3453−3461.
(8) Cabaleiro-Lago, C.; Quinlan-Pluck, F.; Lynch, I.; Dawson, K. A.; Linse, S. *ACS Chem. Neurosci.* **2010**, *1* (4), 279−287.
(9) Linse, S.; Cabaleiro-Lago, C.; Xue, W.-F.; Lynch, I.; Lindman, S.; Thulin, E.; Radford, S. E.; Dawson, K. A. *Proc. Natl. Acad. Sci. U. S. A.* **2007**, *104* (21), 8691−8696.
(10) Javed, I.; Sun, Y.; Adamcik, J.; Wang, B.; Kakinen, A.; Pilkington, E. H.; Ding, F.; Mezzenga, R.; Davis, T. P.; Ke, P. C. *Biomacromolecules* **2017**, *18* (12), 4316−4322.
(11) Morales, R.; Moreno-Gonzalez, I.; Soto, C. *PLoS Pathog.* **2013**, *9* (9), e1003537.
(12) Maury, C. *J. Intern. Med.* **2009**, *265* (3), 329−334.
(13) Morales, R.; Estrada, L. D.; Diaz-Espinoza, R.; Morales-Scheihing, D.; Jara, M. C.; Castilla, J.; Soto, C. *J. Neurosci.* **2010**, *30* (13), 4528−4535.
(14) Lee, J.; Bhak, G.; Lee, J. H.; Park, W.; Lee, M.; Lee, D.; Jeon, N. L.; Jeong, D. H.; Char, K.; Paik, S. R. *Angew. Chem., Int. Ed.* **2015**, *54* (15), 4571−4576.
(15) García-Ayllón, M.-S.; Small, D. H.; Avila, J.; Sáez-Valero, J. *Front. Mol. Neurosci.* **2011**, *4*, 1−9.
(16) Krotee, P.; Rodriguez, J. A.; Sawaya, M. R.; Cascio, D.; Reyes, F. E.; Shi, D.; Hattne, J.; Nannenga, B. L.; Oskarsson, M. E.; Philipp, S. *eLife* **2017**, *6*, e19273.
(17) Adamcik, J.; Jung, J.-M.; Flakowski, J.; De Los Rios, P.; Dietler, G.; Mezzenga, R. *Nat. Nanotechnol.* **2010**, *5* (6), 423−428.
(18) Nyström, G.; Fong, W.-K.; Mezzenga, R. *Biomacromolecules* **2017**, *18* (9), 2858−2865.
(19) Bolisetty, S.; Mezzenga, R. *Nat. Nanotechnol.* **2016**, *11* (4), 365.
(20) Li, C.; Adamcik, J.; Mezzenga, R. *Nat. Nanotechnol.* **2012**, *7* (7), 421−427.
(21) Cedervall, T.; Lynch, I.; Lindman, S.; Berggård, T.; Thulin, E.; Nilsson, H.; Dawson, K. A.; Linse, S. *Proc. Natl. Acad. Sci. U. S. A.* **2007**, *104* (7), 2050−2055.
(22) Fu, Z.; Luo, Y.; Derreumaux, P.; Wei, G. *Biophys. J.* **2009**, *97* (6), 1795−1803.
(23) Castagnola, V.; Zhao, W.; Boselli, L.; Lo Giudice, M.; Meder, F.; Polo, E.; Paton, K.; Backes, C.; Coleman, J.; Dawson, K. *Nat. Commun.* **2018**, *9* (1), 1577.
(24) Monopoli, M. P.; Åberg, C.; Salvati, A.; Dawson, K. A. *Nat. Nanotechnol.* **2012**, *7* (12), 779−786.
(25) Matsuura, K.; Saito, T.; Okazaki, T.; Ohshima, S.; Yumura, M.; Iijima, S. *Chem. Phys. Lett.* **2006**, *429* (4), 497−502.
(26) Gosal, W. S.; Clark, A. H.; Pudney, P. D.; Ross-Murphy, S. B. *Langmuir* **2002**, *18* (19), 7174−7181.
(27) Sethuraman, A.; Vedantham, G.; Imoto, T.; Przybycien, T.; Belfort, G. *Proteins: Struct., Funct., Genet.* **2004**, *56* (4), 669−678.
(28) Roach, P.; Farrar, D.; Perry, C. C. *J. Am. Chem. Soc.* **2005**, *127* (22), 8168−8173.
(29) Lara, C.; Adamcik, J.; Jordens, S.; Mezzenga, R. *Biomacromolecules* **2011**, *12* (5), 1868−1875.
(30) Li, C.; Bolisetty, S.; Chaitanya, K.; Adamcik, J.; Mezzenga, R. *Adv. Mater.* **2013**, *25* (7), 1010−1015.
(31) The Lancet. Alzheimer's disease: expedition into the unknown. *Lancet* **2016**, *388* (10061), 2713.
(32) Howe, K.; Clark, M. D.; Torroja, C. F.; Torrance, J.; Berthelot, C.; Muffato, M.; Collins, J. E.; Humphray, S.; McLaren, K.; Matthews, L.; et al. *Nature* **2013**, *496* (7446), 498.
(33) Kalueff, A. V.; Stewart, A. M.; Gerlai, R. *Trends Pharmacol. Sci.* **2014**, *35* (2), 63−75.
(34) Best, J.; Alderton, W. K. *Neuropsych. Dis. Treat.* **2008**, *4* (3), 567−576.
(35) Das, P. K.; Dean, D. N.; Fogel, A. L.; Liu, F.; Abel, B. A.; McCormick, C. L.; Kharlampieva, E.; Rangachari, V.; Morgan, S. E. *Biomacromolecules* **2017**, *18* (10), 3359−3366.
(36) Munishkina, L. A.; Cooper, E. M.; Uversky, V. N.; Fink, A. L. *J. Mol. Recognit.* **2004**, *17* (5), 456−464.
(37) Cabaleiro-Lago, C.; Szczepankiewicz, O.; Linse, S. *Langmuir* **2012**, *28* (3), 1852−1857.
(38) Okada, A.; Sano, K.; Nagata, K.; Yasumasu, S.; Ohtsuka, J.; Yamamura, A.; Kubota, K.; Iuchi, I.; Tanokura, M. *J. Mol. Biol.* **2010**, *402* (5), 865−878.
(39) Nedumpully-Govindan, P.; Ding, F. *Sci. Rep.* **2015**, *5*, 8240.
(40) Ge, X.; Kakinen, A.; Gurzov, E. N.; Yang, W.; Pang, L.; Pilkington, E. H.; Govindan-Nedumpully, P.; Chen, P.; Separovic, F.; Davis, T. P.; et al. *Chem. Commun.* **2017**, *53* (68), 9394−9397.
(41) Raleigh, D.; Zhang, X.; Hastoy, B.; Clark, A. *J. Mol. Endocrinol.* **2017**, *59* (3), R121−R140.
(42) Sivanesam, K.; Shu, I.; Huggins, K. N.; Tatarek-Nossol, M.; Kapurniotu, A.; Andersen, N. H. *FEBS Lett.* **2016**, *590* (16), 2575−2583.
(43) Wijesekara, N.; Ahrens, R.; Wu, L.; Ha, K.; Liu, Y.; Wheeler, M.; Fraser, P. *Diabetes, Obes. Metab.* **2015**, *17* (10), 1003−1006.
(44) Wang, H.; Abedini, A.; Ruzsicska, B.; Raleigh, D. P. *Biochemistry* **2014**, *53* (37), 5876−5884.
(45) Potter, K. J.; Scrocchi, L. A.; Warnock, G. L.; Ao, Z.; Younker, M. A.; Rosenberg, L.; Lipsett, M.; Verchere, C. B.; Fraser, P. E. *Biochim. Biophys. Acta, Gen. Subj.* **2009**, *1790* (6), 566−574.
(46) Scrocchi, L. A.; Chen, Y.; Waschuk, S.; Wang, F.; Cheung, S.; Darabie, A. A.; McLaurin, J.; Fraser, P. E. *J. Mol. Biol.* **2002**, *318* (3), 697−706.
(47) Westermark, P.; Grimelius, L. *Acta Pathol. Microbiol. Scand., Sect. A* **1973**, *81* (3), 291−300.
(48) Donnini, S.; Solito, R.; Cetti, E.; Corti, F.; Giachetti, A.; Carra, S.; Beltrame, M.; Cotelli, F.; Ziche, M. *FASEB J.* **2010**, *24* (7), 2385−2395.
(49) Okada, A.; Sano, K.; Nagata, K.; Yasumasu, S.; Ohtsuka, J.; Yamamura, A.; Kubota, K.; Iuchi, I.; Tanokura, M. *J. Mol. Biol.* **2010**, *402* (5), 865−878.
(50) Xia, T.; Zhao, Y.; Sager, T.; George, S.; Pokhrel, S.; Li, N.; Schoenfeld, D.; Meng, H.; Lin, S.; Wang, X.; Wang, M.; Ji, Z.; Zink, J. I.; Mädler, L.; Castranova, V.; Lin, S.; Nel, A. E. *ACS Nano* **2011**, *5* (2), 1223−1235.
(51) Huang, S. M.; Xu, F.; Lam, S. H.; Gong, Z.; Ong, C. N. *Mol. BioSyst.* **2013**, *9* (6), 1372−1380.
(52) Lin, S.; Zhao, Y.; Ji, Z.; Ear, J.; Chang, C. H.; Zhang, H.; Lowkam, C.; Yamada, K.; Meng, H.; Wang, X.; et al. *Small* **2013**, *9* (9−10), 1776−1785.
(53) Lee, J.; Bhak, G.; Lee, J. H.; Park, W.; Lee, M.; Lee, D.; Jeon, N. L.; Jeong, D. H.; Char, K.; Paik, S. R. *Angew. Chem., Int. Ed.* **2015**, *54* (15), 4571−4576.
(54) Amit, M.; Yuran, S.; Gazit, E.; Reches, M.; Ashkenasy, N. *Adv. Mater.* **2018**, 1707083.
(55) Gao, N.; Sun, H.; Dong, K.; Ren, J.; Duan, T.; Xu, C.; Qu, X. *Nat. Commun.* **2014**, *5*, 3422.
(56) Geng, J.; Li, M.; Ren, J.; Wang, E.; Qu, X. *Angew. Chem., Int. Ed.* **2011**, *50* (18), 4184−4188.
(57) Li, M.; Yang, X.; Ren, J.; Qu, K.; Qu, X. *Adv. Mater.* **2012**, *24* (13), 1722−1728.

DOI: 10.1021/acs.nanolett.8b02446
Nano Lett. 2018, 18, 5797−5804